Analysis of interplanetary Lyman-alpha line profile with a hydrogen absorption cell - Theory of the Doppler angular spectral scanning method

Jean-Loup Bertaux, Rosine Lallement

Astron. Astrophys. 140, 230–242 (1984)

ASTRONOMY AND ASTROPHYSICS

Analysis of interplanetary Lyman-alpha line profile with a hydrogen absorption cell: theory of the Doppler angular spectral scanning method

J.L. Bertaux and R. Lallement

Service d'Aéronomie du C.N.R.S., F-91370 Verrières-le-Buisson, France

Received October 17, 1983; accepted July 12, 1984

Summary. The use of a hydrogen absorption cell as a means of diagnostic for interstellar hydrogen is described. Through resonance scattering of solar Lyα photons, the interstellar atoms penetrating into the solar system present a Lyα emission the profile of which is an image of their velocity distribution. From the study of hydrogen Lyα profiles the temperature T of the interstellar hydrogen and the three components of the relative velocity vector V_w can be determined. The case in which the velocity distribution of H atoms in the interplanetary medium is the same Maxwell-Boltzmann distribution as at infinity (the uniform gaussian case) is completely described. The hydrogen absorption cell is used at a fixed optical thickness $\tau \simeq 10$ (shown to be an optimal choice) and the analysis of the Lyα profile is made by modulating the Doppler shift between the source and the observer. This modulation is simply obtained by looking at different directions of the sky, providing a Doppler angular spectral scanning of the Lyα profile. The absorption pattern on the whole celestial sphere is shown to look like a "crunched apple" or a peanut, with a symmetry of revolution around the relative velocity vector between the observer and the interstellar hydrogen. From this absorption pattern it is shown how T and V_w can be derived directly from the observations, with a purely geometrical method requiring no modeling. When observations are limited to a scan plane perpendicular to the Earth-Sun line, it is shown how three observations at different places in the solar system can be used to determine completely T and V_w, even if some galactic background emission is superimposed to the interplanetary Lyα.

In a companion paper (this issue), this method is applied to five sets of observations made with the soviet satellites Prognoz 5 and Prognoz 6, giving a first approximation of the values of T and V_w, but yielding also organized departures from the uniform gaussian case.

Key words: interstellar medium – interstellar hydrogen – Lyman-alpha – gas absorption cell

1. Introduction

When neutral hydrogen and helium atoms of the local interstellar medium (LISM) are flowing in the solar system, they can be observed through resonance scattering of solar H Lyα (121.6 nm) and He 58.4 nm radiation. The interaction with the solar environment includes in particular a gravitational focusing of helium atoms and a cavity of ionization in the hydrogen distribution, mainly due to charge exchange with solar wind protons. Therefore, observations of interstellar gas in the solar system convey information on three subjects: the unperturbed LISM (at $\simeq 10^3$ A.U. from the Sun), a possible partial interaction at the heliopause boundary (Ripken and Fahr, 1983), and the flux of the ionizing solar wind. These three subjects are of interest to a wide community of scientists, who may not be very familiar with the methods which are used to investigate these topics from interplanetary observations. The purpose of this paper is to present the basic principles of a powerful diagnostic method, the line shape analysis of H Lyα emission with a hydrogen absorption cell used in a mode of Doppler angular spectral scanning.

The motion of the solar system relative to the nearby stars forming the local frame of reference is characterized by a velocity vector V_a of 20 kms^{-1} in the Apex direction, $\alpha = 271°$ and $\delta = 30°$ (equatorial coordinates). Before 1970 it was expected that this motion would cause neutral matter of the LISM to be swept into the solar system. In particular, hydrogen and helium atoms were predicted to penetrate deeply in the solar system (Blum and Fahr, 1970). This prediction was confirmed with the observations of extraterrestrial H Lyα (Bertaux and Blamont, 1971; Thomas and Krassa, 1971) and later with the observations of He emissions at 58.4 nm (Weller and Meier, 1974). However, these observations indicated that the solar system travels through the interstellar gas with a velocity vector V_w, pointed in the direction V_w, different from the Apex direction by 50°. That is to say that the interstellar medium is moving relative to the nearby stars with a velocity vector $V_t = V_a - V_w$; this motion has been called the "interstellar wind".

The LISM is also characterized by the temperature T and the densities n_∞(H) and n_∞(He) outside the heliosphere. With a model describing the interaction between the solar system and the LISM, one can compute, for a given set of parameters V_w, T, and n_∞, the distribution of n(H) and n(He) in the solar system, as well as the intensity distribution of HLα (121.6 nm) and He(58.4 nm) resonantly scattered solar radiation. From the comparison of computed and measured intensities, one hopes to derive the parameters n_∞, V_w, T.

The direction of V_w can either be determined by the location of the downwind helium focusing cone whose axis is the vector $-V_w$, or by the annual parallactic motion of the maximum intensity direction at Lyα (in the upwind region). The temperature T influences the intensity distribution around the downwind axis

Send offprint request to: J.L. Bertaux

$-V_w$. In the case of helium, the thermal velocity spread smears the sharp maximum which is expected from gravitational focusing. For hydrogen, solar Lyα radiation pressure prevents gravitational focusing and there should be no hydrogen downwind (because of ionization), if it were not for the filling in of this region by the H thermal velocity spread.

Densities n_∞ are derived from the absolute value of the intensity, provided that the exciting solar flux F_s is known, as well as V_w, T and the ionization rate.

This investigation method, that could be called the "photometric pattern method", has been used on several space experiments. The Naval Research Laboratory group conducted a series of helium experiments on OSO-8, STP-72, and SOLRAD spacecrafts. The direction of the wind was determined to be $\alpha = 252°$, $\delta = -15°$ (Weller and Meier, 1974). Then the range of parameters T, V_w was progressively narrowed to $T = 9{,}000$–$15{,}000$ K and $V_w = 22$–$28\ \mathrm{km\,s^{-1}}$ (Weller and Meier, 1981). Broadfoot and Kumar (1978) derived from Mariner 10 observations velocities of 15–$30\ \mathrm{km\,s^{-1}}$ and temperatures of 5,000–30,000 K. More recently, Dalaudier et al. (1984), analysing helium data from Prognoz-6 spacecraft, reached a range of $T \simeq 11{,}000$–$24{,}000$ K and $V_w \simeq 23$–$30\ \mathrm{km\,s^{-1}}$.

Hydrogen investigation using the photometric pattern method found first the direction of the wind V_w to be $\alpha = 265°$, $\delta = -15°$ (Bertaux and Blamont, 1971), and temperatures in the range 1,000–15,000 K (Bertaux et al., 1972; Thomas, 1972). One might however question seriously the reality of the differences found between hydrogen and helium concerning the wind direction and temperature, because of several shortcomings of the photometric pattern method. One of them is that the light flux of the sun at Lyα and 58.4 nm is not isotropic, which modifies the shape of the photometric pattern in respect to the isotropic case assumed in the models. A more severe problem concerns the ionization rate of H atoms. The ionized cavity in the downwind direction can be filled partially either by a larger temperature T or by a lower ionization rate, and since the accurate value of this parameter is not well known, the hydrogen temperature cannot be accurately determined from the Lyα intensity pattern. Furthermore, the main source of ionization is charge exchange with solar wind protons, which flux is not known outside the ecliptic plane. A non isotropic solar wind would modify substantially the Lyα pattern, preventing to determine accurately the direction of the incoming flow (Bertaux and Blamont, 1971; Joselyn and Holzer, 1975). Indeed, Kumar and Broadfoot (1979) found on Mariner 10 observations some evidence that the solar wind is not isotropic.

In view of these shortcomings of the photometric pattern method, spectrometric informations can yield independant and crucial informations, because through Doppler effect the line shape of the resonant emission is an image of the velocity distribution of atoms, projected on and integrated along the line of sight. In the case of H Lyα, the solar line is wide enough that it may be considered as flat on the interval of sun radial velocities of H atoms, and the line shape is strictly the image of the projected velocity distribution. In addition, since the solar Lyα radiation pressure is approximately in equilibrium with solar gravitation, the H velocity distribution may be not too much modified from its Maxwell Boltzmann shape at infinity.

For helium, two effects are playing an important role. First the velocity distribution of He atoms is strongly modified by the solar gravitation; second, the solar line width is small enough that the resonant line shape is modified in respect to the velocity distribution, since atoms with a large Doppler effect respective to the sun will be excited at a lower rate, and may even not be excited at all.

All these effects can be taken into account in predictive spectrometric models of line shapes of H and He emission; see for instance Meier (1977) and Wallis and Wallis for an approximate formulation (1979). But what really lacked for a long time were spectrometric measurements of high quality.

With the UV spectrometer of Copernicus observatory, Adams and Frisch (1977) obtained a weak line of the LISM H Lyα emission, in only one direction of sight after six days of integration. They found a Doppler shift of $22 \pm 3\ \mathrm{km\,s^{-1}}$ and a width corresponding to 20,000 K or less. More powerful is the use of resonance absorption cells associated to photometers, the theory of which will be described below.

Up to now, helium cells have been used mainly on rocket payloads, with the two limitations of short integration time and heavy contamination by geocoronal helium emission. Such a system is for instance described in Freeman et al., 1976 and Fahr et al., 1977. In this last experiment, due to the limited measurement time, only an upper limit of the interplanetary emission of 7 to 10 Rayleigh could be obtained. Better results were obtained during the Apollo-Soyuz Test Project, as discussed later (Freeman et al., 1980).

Hydrogen absorption cells have been used both for the study of H planetary coronae (Earth, Bertaux, 1978; Venus, Bertaux et al., 1978; Mars, Babichenko et al., 1977) and for the study of interplanetary H Lyα emission. The first use of an H absorption cell on the interplanetary emission was made during the cruise phase of the Mars-7 mission and indeed some of the emission was absorbed by the cell (Bertaux et al., 1976). However, the orientation of the probe was not known precisely, and only a temperature range of 6,000–13,000 K was given, still much narrower than earlier determinations based on the photometric pattern method. Finally, a hydrogen cell was placed on board two Earth orbiting satellites, Prognoz 5 in 1976 and Prognoz 6 in 1977, and provided an estimate range for the temperature of 7,800–9,800 K (Bertaux et al., 1977).

The European Space Agency had decided to fly both hydrogen and helium absorption cells on the out-of-ecliptic mission ISPM. Though it was a part of the European payload complement, this experiment was assigned to the US spacecraft of the ISPM mission, which was unfortunately cancelled later by NASA. Meanwhile, the analysis of Prognoz large set of data has progressed substantially, and the results of this 12 yr research program will be presented in a series of four papers. In the present paper (paper 1) we present the basic principles of the theory of the use of a resonance absorption cell as a diagnostic tool for the interstellar/interplanetary gas. A simple case is considered here, in which the velocity distribution of H atoms is not modified by the solar interaction: this is the uniform gaussian case. We describe a method for retrieving the parameters T and V_w directly from the data, without any modeling. In a companion paper (Lallement et al., 1984, this issue), this method is applied to Prognoz results, and indeed a first estimate of T and V_w can be fairly well achieved. However, the results present substantial deviations from the predictions of the simple uniform gaussian case. The effect of a possible contamination by some additional galactic background emission in the band-width of the instrument is examined and it is shown that it cannot explain the deviations. These deviations are the signature that indeed, the H atoms velocity distribution is modified by the solar environment, and the uniform gaussian model can be used only for a first estimate.

In paper 3 (Lallement et al., in preparation) we will examine thoroughly how the velocity distribution is modified by solar wind and EUV ionization, and by the unbalanced effect of solar gravitation and solar Lyα radiation pressure. The effect on

reduction factor measurements will be fully described, with the results of a sophisticated computer code.

In a fourth paper (Bertaux et al., in preparation) the Prognoz missions will be presented and the Lyα photometer/hydrogen cell will be described, together with the data reduction procedure. The results will be compared with the model of paper 3 to extract a more accurate determination of T and V_w, and to determine the value of parameters describing the interaction with the solar environment.

2. Theory of a gas absorption cell

A typical gas absorption cell experiment consists of a crude spectral rejection system, a detector sensitive to the resonance radiation, and the absorption cell itself. In the case of helium, the detector is usually a channel electron multiplier, the cell has two windows of metal thin film (Al or Sn), and the optical thickness τ of helium in the cell is controlled by filling and evacuation of helium (for a more detailed description of a rocket instrument flown for an analysis of the He I 58.4 nm solar line, see Delaboudinière and Carabetian, 1975; for the results, see Delaboudinière and Crifo, 1976; Delaboudinière, 1981).

The Lyman α photometer flown on Prognoz 5 and Prognoz 6 consisted of a solar blind photomultiplier as the detector, placed behind a hydrogen absorption cell, which is a teflon coated glass vessel with two MgF_2 windows. The entrance window is a lens, which focus is between the cell and the PM tube. A rectangular hole at the focus defines a field of view of $1.3 \times 3°$. The exit window of the cell is covered with an evaporated thin film filter, which defines a total bandwidth of ~ 10 nm centered at Lyman α. In the following, it will be assumed (unless otherwise specified) that the only radiation seen by the detector is resonance radiation from hydrogen (or helium) atoms.

The cell is sealed and permanently filled with H_2 at a few mm Hg (a few hundreds Pascal) pressure. A tungsten filament placed inside the cell can be heated electrically, and H_2 molecules touching the filament are dissociated into atoms, creating an optical thickness τ of atomic hydrogen. When the filament is switched off, there is immediate (within $\simeq 0.05$ s) recombination into molecules. Whereas H_2 is totally transparent to Lα, when the optical thickness τ is created inside the cell, incoming photons lying near the resonance line center are scattered away from the direct beam and absorbed on the cell walls. The transmission function $T(\lambda)$ of the cell is, in the reference frame of the cell and as a function of wavelength λ:

$$T(\lambda) = \exp[-\tau H(a, v)], \tag{1}$$

where $H(a, v)$ is the unnormalized Voigt function as given by Harris (1948):

$$H(a, v) = \frac{a}{\pi} \int_{-\infty}^{+\infty} \frac{e^{-y^2}}{a^2 + (v - y)^2}\, dy, \tag{2}$$

where $a = 2.7\ 10^{-3}$ is the ratio of natural to Doppler width $\Delta\lambda_c$, and

$$v = \frac{\lambda - \lambda_0}{\Delta\lambda_c}, \quad \Delta\lambda_c = \frac{\lambda_0}{c}\left(\frac{2kT_c}{m}\right)^{1/2}.$$

m is the mass of the hydrogen (or helium) atom, T_c the temperature of the gas in the cell, which is equal to the instrument temperature because of numerous collisions of atoms with the cell walls, and is $T_c \simeq 300$ K.

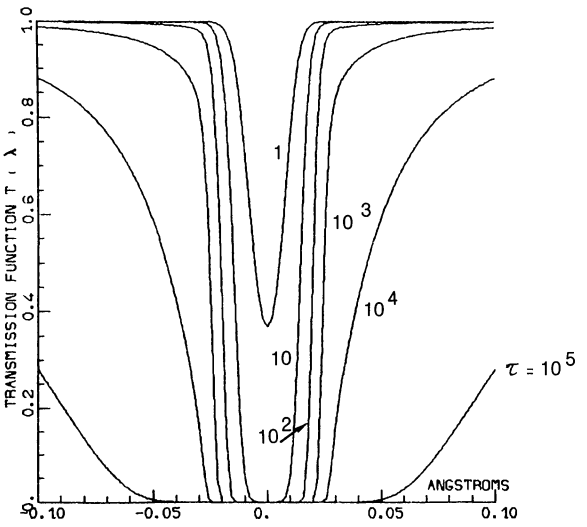

Fig. 1. The optical transmission $T(\lambda)$ of a hydrogen absorption cell is displayed as a function of wavelength distance to line center $\lambda - \lambda_0$, for various values of the optical thickness τ ranging from 1 to 10^5. The wings of the Voigt profile begin to absorb significantly for $\tau = 10^3$. For $\tau = 10$, which is the optical thickness of the cell used for the study of interplanetary Lyα emission, the sides of the absorption profile are very steep. Absorption is complete at line center

The transmission function is symmetrical in respect to λ_0, the resonance wavelength, and is displayed in Fig. 1 for various values of τ between 1 and 10^5. Because of saturation the transmission function does not change very much between $\tau = 10$ and $\tau \simeq 10^3$, whereas for higher values of τ the wings of the absorption line become important. If $f(\lambda)$ is the spectral profile of the emission to be analyzed, the detector signal, which integrates over wavelength the whole spectrum of the line, is:

$$I_0 = C \int f(\lambda)\, d\lambda \tag{3}$$

when the cell is empty (helium) or switched off (hydrogen), where C accounts for the calibration of the instrument. When the cell is activated with an optical thickness τ (filled with helium, or switched on for H), the signal recorded by the detector is:

$$I(\tau) = C \int f(\lambda)\, T(\lambda)\, d\lambda. \tag{4}$$

The ratio $R = \dfrac{I}{I_0}$ is called the reduction factor:

$$R(\tau) = \frac{I(\tau)}{I_0} = \frac{\int f(\lambda) \exp[-\tau H(a, v)]\, d\lambda}{\int f(\lambda)\, d\lambda} \tag{5}$$

whereas the absorption $A(\tau)$ is $1 - R(\tau)$.

From Eq. (5) it is clear that, from a series of measurements $R(\tau)$ of the same emission profile $f(\lambda)$ with various values of τ, one can inverse the integral of second member at numerator, and find the function $f(\lambda)$, the spectral profile to be analyzed. Several methods for numerical inversion of (5) have been investigated thoroughly, and successfully aplied to the line profile measurement of solar He I 58.4 nm by Delaboudinière (1981). This method, that could be called the τ variation method, is adequate for helium, because it is a monoatomic gas and therefore it is relatively easy to obtain large values of τ in the absorption cell, necessary to explore a substantial wavelength range around λ_0.

On the contrary, for hydrogen this method is more difficult to apply, since large values of τ would require a high temperature of the tungsten filament, and a high electrical power is sometimes

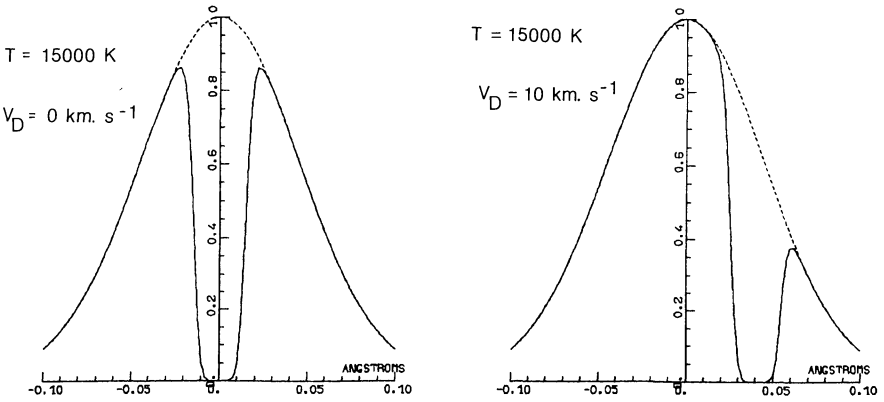

Fig. 2. The effect of absorption by a cell with $\tau = 10$ and a cell temperature of 300 K on a gaussian line profile at $T = 15\,000$ K is shown for two Doppler shift velocities, $V_D = 0$ and $V_D = 10$ km s^{-1}. The dashed curve is the profile before absorption. The solid line is the line profile after absorption. The area under the solide line, divided by the total area under the non absorbed line, is the reduction factor R

prohibitive on long duration space missions. At present, the largest optical thickness obtained is of the order of $\simeq 600$ with a power of 30 watts in one instrument prepared for the First Spacelab mission, and devoted to the study of hydrogen and deuterium in the Earth's atmosphere. But from Fig. 1 it is seen that the wavelength range explored with $\tau = 600$ is not very much larger than for $\tau = 10$, which can be obtained easily with $\simeq 3$ watts of electrical power.

Another way to analyze the emission profile is to use a constant value of τ and a variable Doppler shift $\Delta\lambda_D$ between the instrument and the emission source. The reduction factor is now a function of $\Delta\lambda_D$:

$$R(\Delta\lambda_D) = \frac{I(\Delta\lambda_D)}{I_0} = \frac{\int f(\lambda - \Delta\lambda_D)\, T(\lambda)\, d\lambda}{\int f(\lambda)\, d\lambda}. \tag{6}$$

On Fig. 2 is displayed for $f(\lambda)$ a gaussian Lα profile with a temperature emission $Te = 15{,}000$ K, modified by the transmission $T(\lambda)$ acting at two different Doppler shifts $\Delta\lambda_D$. The detector signal $I(\Delta\lambda_D)$, when the cell is activated, is proportional to the area under the solid lines, and this area is the convolution product of profile $f(\lambda)$ by the transmission function $T(\lambda)$. The absorption cell may be in this case regarded as a "negative" spectrometer with a resolution equal to the equivalent width of absorption, $W = 30$ mÅ or 7.4 km s^{-1} for $\tau = 10$ for instance.

From a series of measurements obtained at various values of Doppler shift $\Delta\lambda_D$, integral (6) can be deconvoluted and the line profile $f(\lambda)$ retrieved with a spectral resolution even better than W, depending on the signal to noise ratio.

This method could be for instance applied with an Earth's orbiting spacecraft looking at a source in a constant direction, with the orbiting velocity projected on the line of sight providing the variable Doppler shift. But, even at low altitudes where the velocity is maximum at 8 km s^{-1}, the total wavelength range explored is only 0.065 Å at Lα, which is not very much; and geocoronal Lα contamination in this case is a severe limitation for observations of weak extra-terrestrial Lα emissions like the interplanetary emission.

However, by looking in the sky at different directions of sight $\boldsymbol{u}$ a larger wavelength exploration is obtained owing to the orbital velocity $\boldsymbol{V}_s$ of the spacecraft in the solar system, combined with the wind velocity $\boldsymbol{V}_w$ of $\simeq 20$–25 km s^{-1}. The total relative velocity between the spacecraft and the H interstellar flow is $\boldsymbol{V}_R = \boldsymbol{V}_s + \boldsymbol{V}_w$. For Prognoz satellites, which spend most of their time at large distances of the Earth, and have at apogee a low orbital velocity which can be neglected, $V_s \simeq V_E = 30$ km s^{-1}, where V_E is the Earth's orbital velocity.

The Doppler effect in the line of sight $\boldsymbol{u}$ is:

$$\Delta\lambda_D = \frac{\lambda_0}{c} V_R \mathrm{Cos}(\boldsymbol{V}_R, \boldsymbol{u}) = \frac{\lambda_0}{c} V_R \mathrm{Cos}\,\alpha = \frac{\lambda_0}{c} V_D. \tag{7}$$

α being the angle between $\boldsymbol{u}$ and $\boldsymbol{V}_R$. Therefore, looking at various angles α provides a scanning of the emission line through the variation of $\Delta\lambda_D$. Again, a series of measurements $R(\Delta\lambda_D)$ can be deconvoluted to retrieve the spectral shape of $f(\lambda)$. This method can be described as the Doppler angular spectral scanning method, and will be elaborated below for various typical situations of space missions. It should be noted that, since the reduction factor $R(\Delta\lambda_D)$ is a relative quantity, it is not required that the absolute intensity I_0 be identical in all directions. It is only required that the spectral shape $f(\lambda)$ be the same in all directions, or in the sky region where it is applied.

For the case of a simple gaussian corresponding to a temperature T_e of the interplanetary hydrogen, the reduction factor can be expressed as an integral, function of T_e, the Doppler Shift $V_D = V_r \cos\alpha$ and the optical thickness τ:

$$R(T_e, V_D, \tau) \tag{8}$$
$$= \frac{1}{\Delta\lambda_e \sqrt{\pi}} \int_{-\infty}^{+\infty} \exp\left[-\frac{(\Delta\lambda_D - \Delta\lambda)^2}{\Delta\lambda_e^2} - \tau H(a, v) \right] d\lambda$$

in which

$$\Delta\lambda_e = \frac{\lambda_0}{c}\left(\frac{2kT_e}{m}\right)^{1/2} \quad \text{and} \quad \Delta\lambda = \lambda - \lambda_0.$$

Instead of considering the reduction factor, one can consider the absorption, which is the complement of the reduction factor:

$$A(V_D) = 1 - R(V_D).$$

It corresponds to the proportion of photons absorbed by the cell, which lie within the narrow bandwidth of the cell ($\simeq 30$ mÅ for $\tau = 10$), therefore which have been emitted at small radial velocities respective to the cell. As was said before, the H cell is functionning as a "negative" spectrometer, if R is the signal. If $A = 1 - R$ is considered to be the signal of such a spectrometer, the transfer function of this spectrometer is $1 - T(\lambda)$. When the Doppler Shift V_D is scanned, the output signal $A(V_D)$ is the convolution of the

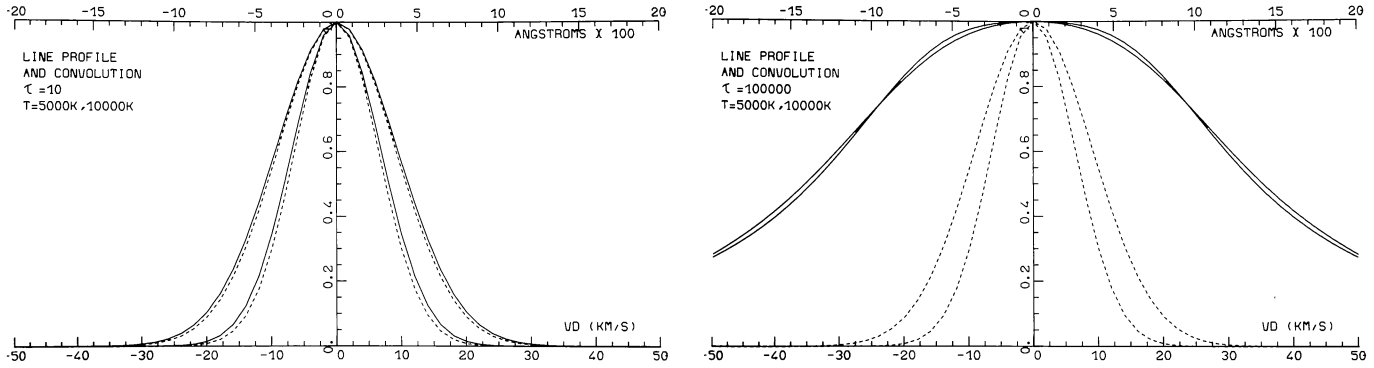

a b

Fig. 3a and b. A comparison is presented between a pure gaussian profile $f(\lambda)$ (solid lines) and the absorption $A(V_D)$ by the cell of the profile $f(\lambda)$ as a function of the Doppler shift V_D, or of the equivalent wavelength shift. The curves $A(V_D)$ have been normalized to unity for $V_D = 0$, as the curves $f(\lambda)$. The two cases of emission temperatures $T = 5000$ K and $T = 10{,}000$ K are shown. For an optical thickness of 10 (curve **a**) the absorption shape is nearly identical to the emission profile (in fact, only very slightly enlarged). The Doppler angular scanning with $\tau = 10$ provides a spectral scanning of very good quality. For an optical thickness of 10^5 (curve **b**) the absorption shape $A(V_D)$ is only slightly related to the emission temperature, and is in fact very similar to the absorption function $T(\lambda)$ (Fig. 1), whatever is the temperature (for $T \lesssim 15{,}000$ K)

spectral profile $f(\lambda)$ by the transfer function $1 - T(\lambda)$:

$$A(V_D) \equiv A(\Delta\lambda_D) = \frac{I_0 - I(\Delta\lambda_D)}{I_0}$$

$$= \frac{\int f(\lambda - \Delta\lambda_D)\,[1 - T(\lambda)]\,d\lambda}{\int f(\lambda)\,d\lambda}\,.$$

The curve $A(V_D)$ can be plotted as a function of the Doppler shift velocity V_D, which is equivalent to a wavelength scale ($10\,\mathrm{km\,s^{-1}} = 40.5$ mÅ). In Fig. 3a and b are shown (dashed lines) two gaussian profiles at 5,000 and 10,000 K, and the corresponding curves $A(V_D)$ (solid lines), for two values of τ: 10 and 10^5. All curves have been normalized to unity at line center. In the case $\tau = 10$ (Fig. 3a), the curve $A(V_D)$ is quite similar to the gaussian spectral profile, and is only very slightly enlarged. Practically the curve $A(V_D)$ is the spectral profile $f(\lambda)$ to be analyzed with the hydrogen cell, and this would be true for any profile shape, provided it is substantially wider than the width of the transmission function.

On the contrary, when $\tau = 10^5$ (Fig. 3b), the two curves $A(V_D)$ for 5,000 and 10,000 K are quite identical, and very difficult to discriminate. This is because the width of the absorption function (Fig. 1) for $\tau = 10^5$ is now substantially larger than the gaussian profiles (a factor of $\simeq 3$ for $T = 10{,}000$ K). In fact, what happens in this case is that the curve $A(V_D)$, instead of being an image of $f(\lambda)$, as for $\tau = 10$, is now an image of the absorption function of the cell.

It is therefore clear that, in order to analyze gaussian profiles in the range 5,000–10,000 K, a moderate optical thickness $\tau = 10$ is more appropriate than a large optical thickness $\tau = 10^5$.

Returning to the case $\tau = 10$, since the curve $A(V_D)$ is a good image of the spectral profile $f(\lambda)$, it follows that the curve $R(V_D) \equiv 1 - A(V_D)$ is in fact a reversed image of the spectral profile $f(\lambda)$ to be analyzed with the hydrogen cell.

In Fig. 4a, the reduction factor $R(\Delta\lambda_D)$ is plotted as a function of Doppler shift $V_D = V_r \cos\alpha$, for an optical thickness $\tau = 10$ of a hydrogen cell, and a gaussian profile corresponding to various temperatures of the interplanetary hydrogen (from 1,000 to 30,000 K). As expected from Fig. 2, the minimum reduction factor (maximum absorption effect of the cell) is obtained when the Doppler shift V_D is zero. When the Doppler shift is substantially larger than the Doppler width of the line, the absorption effect is vanishing, and the reduction factor $R = 1$. This is the case for $V_D = 20\,\mathrm{km\,s^{-1}}$ and $T = 3{,}000$ K, for instance.

In Fig. 4b are plotted, for the same temperatures, the same curves $R(V_D)$ when $\tau = 10^5$. The values of R when $V_D = 0$ cover a much smaller range $\Delta R \simeq 0.08$, than when $\tau = 10$ ($\Delta R \simeq 0.60$). All curves cross each other around $V_D = 27\,\mathrm{km\,s^{-1}}$ and ΔR does not exceed 0.13, whatever is the value of V_D. Again, it is clear that the use of $\tau = 10^5$ yields a much poorer temperature diagnostic than if $\tau = 10$ is used.

Though we have not performed the same calculations for helium, we suspect that the same conclusion would apply, and this certainly explains, at least partially, why Freeman et al. (1980), using a helium cell with a fixed value $\tau = 10^5$, during the Apollo-Soyouz Test Project were not able to determine what was the temperature of the interplanetary/interstellar helium in the range 5,000 to 20,000 K. Though they clearly measured a substantial absorption, varying with the Doppler Shift, their model calculations were very little sensitive to the temperature, as expected from our analysis for $\tau = 10^5$, and the comparison of the observed absorption to their model yielded a wide range of temperature.

One difficulty to produce a low optical thickness $\tau = 10$ in a helium cell is, as it is a monoatomic gas, the corresponding pressure would be very small and quite difficult to measure and control. One way out is to have a mixture of helium with another buffer gas, like neon, with mixing ratio of He/Ne of $\simeq 10^{-4}$. With a helium cell of 1 cm length at a pressure of 1.4 Torr and an absorption cross section for neon of $0.6\,10^{-17}\,\mathrm{cm^2}$ at 58.4 nm, the continuum attenuation of the intensity due to neon would be only 26 %, which is quite negligible in respect to the low transmission of the windows at this wavelength.

If a large optical thickness $\tau = 10^5$ is required also to have a nearly complete absorption, a second bottle of gas containing pure helium could be used sequentially with the helium neon bottle.

Returning to the case of hydrogen, in Fig. 5 R is plotted as a function of T for $\tau = 10$ and for various values of V_D, and in particular for $V_D = 0$. This last curve is quite useful to determine the temperature, if a measurement of R is obtained when the Doppler shift is zero.

A few more details concerning the H absorption cell have been added in the Appendix.

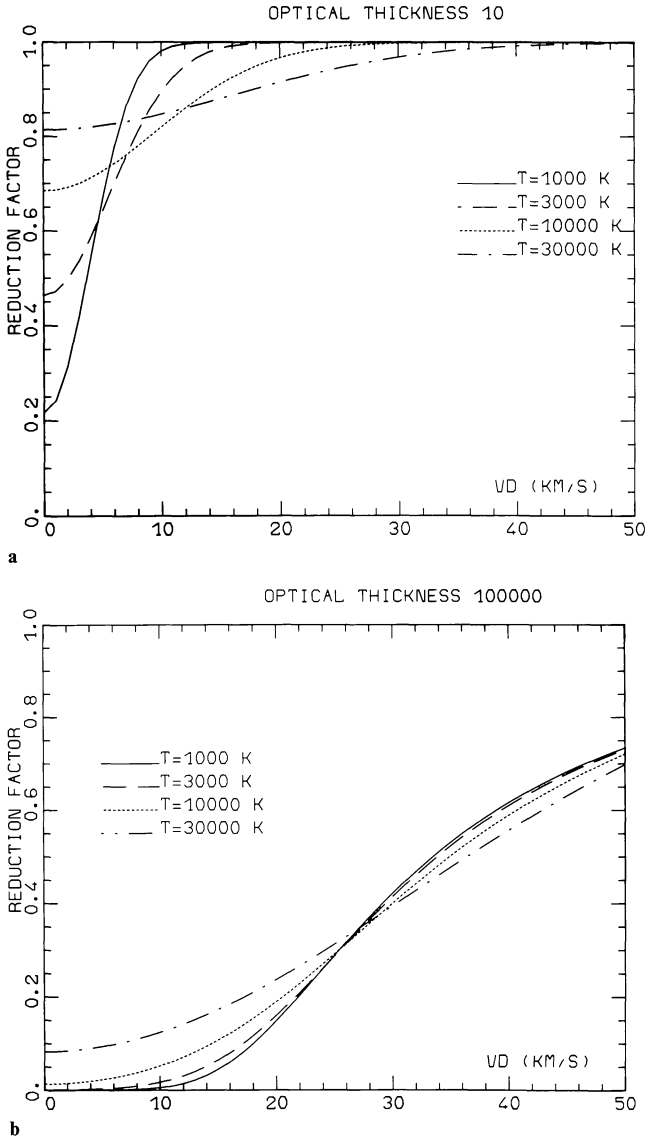

Fig. 4a and b. The reduction factor $R = 1 - A$ is plotted as a function of the Doppler shift V_D along the line of sight for emission Gaussian profiles at $T = 1000, 3000, 10\,000$ and $30\,000$ K. For an optical thickness $\tau = 10$ (curve **a**) the variations of the absorption cover a wide interval in this range of temperatures. On the contrary, for $\tau = 10^5$ (curve 5a) the reduction factor varies in a very small range, which makes difficult to derive an accurate temperature

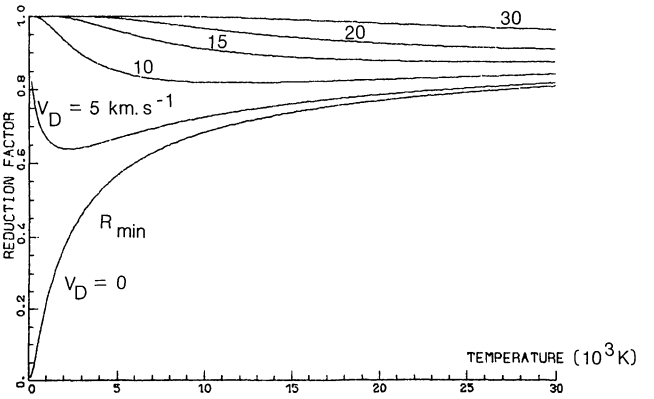

Fig. 5. The reduction factor R is plotted for Gaussian profiles as a function of temperature for various Doppler shifts in km s^{-1}. The curve noted R_{min}, for $V_D = 0$, allows to determine the temperature of the emitting hydrogen from a measurement of the reduction factor at zero Doppler shift

3. Complete mapping of the celestial sphere

Now we describe what would be the variation of the reduction factor R as a function of direction of sight on the whole celestial sphere, as measured from a single position of a spacecraft in the solar system, with a fixed value of the cell optical thickness $\tau = 10$. We will assume that the velocity distribution of H atoms can be described by an isothermal Maxwell Boltzmann distribution with the interstellar gas temperature T, superimposed on the bulk velocity $-\boldsymbol{V}_w$. It is known that the helium atoms velocity distribution is strongly modified by solar gravitation (Meier, 1977; Fahr, 1974; Wallis and Wallis, 1979). In the case of hydrogen, however, the Lα solar radiation pressure is quite strong and more or less balances the solar gravitation. The value of the center line solar flux for which there is an exact balance is $F_s = 3.32\,10^{11}$ phot (cm^2 Å s)$^{-1}$ at 1 A.U., a value which is typical of average solar activity. Therefore, the trajectory of an H atom is practically a straight line in the solar system, and the H velocity distribution of the interstellar gas is not modified when entering the solar system. Deviations from this "equilibrium" assumption will be further discussed in the last section.

From what has been seen in Sect. 2, since the Lα line shape is the same in all directions of sight, the reduction factor R depends only on the angle α between the line of sight $\boldsymbol{u}$ and the vector $\boldsymbol{V}_s + \boldsymbol{V}_w = \boldsymbol{V}_R$. The R pattern will have a symmetry of revolution around axis $\boldsymbol{V}_R$. When $\alpha = 90°$, the Doppler shift is zero, and R reaches its minimum possible value (for a fixed value of T). Such directions lie in the plane perpendicular to the vector $\boldsymbol{V}_R$, which intersects the celestial sphere along a large circle that can be described as the Zero Doppler Shift Circle ZDSC (Bertaux et al., 1976). Therefore, a mapping of the R pattern allows us to determine the position of the ZDSC circle, and the direction of vector $\boldsymbol{V}_R$. Since there is a symmetry of revolution around $\boldsymbol{V}_R$, the whole R pattern may be studied in any half plane containing the V_R axis. In this half-plane, R depends (for a fixed value of T) on the Doppler shift, therefore on angle α and on the value of V_R, as shown by Eq. (7).

In Fig. 6 is represented R computed from Eq. (6), with $\tau = 10$, a gaussian profile $f(\lambda)$ for $T = 10{,}000$ K, and three values of V_R: 10,30 and 50 km s^{-1}. All three curves are symmetrical about $\alpha = 90°$ and have the same value R_{min}, which is an easily computed function of temperature T, and is displayed on Fig. 5 for $V_D = 0$. The reduction factor R depends only on the Doppler shift $V_D = V_R \cos\alpha$. When V_D is large, a small angular scanning around $\alpha = 90°$ is sufficient to displace the H absorption cell profile from the emission line and R rapidly reaches unity. On the contrary, when V_D is small, a much larger angular scanning is needed to get the absorption line away from the emission line. In the extreme situation where V_R would be 0, then the reduction factor R would be at the constant value R_{min}, for all values of α.

The angular width of the region where there is some effect of the H absorption cell depends on the magnitude of V_R. In order to determine V_R from a measurement curve of $R(\alpha)$, a value R_i of $R \neq R_{min}$ is selected, the corresponding value α_i of α is noted. From the curve of Fig. 4a corresponding to the temperature T already determined from R_{min}, and the value R_i, the Doppler shift V_{Di} is determined, and $V_R = V_{Di}/\cos\alpha_i$. Alternately, curves of Fig. 5 can be used. For more precision, several values of R_i can be treated.

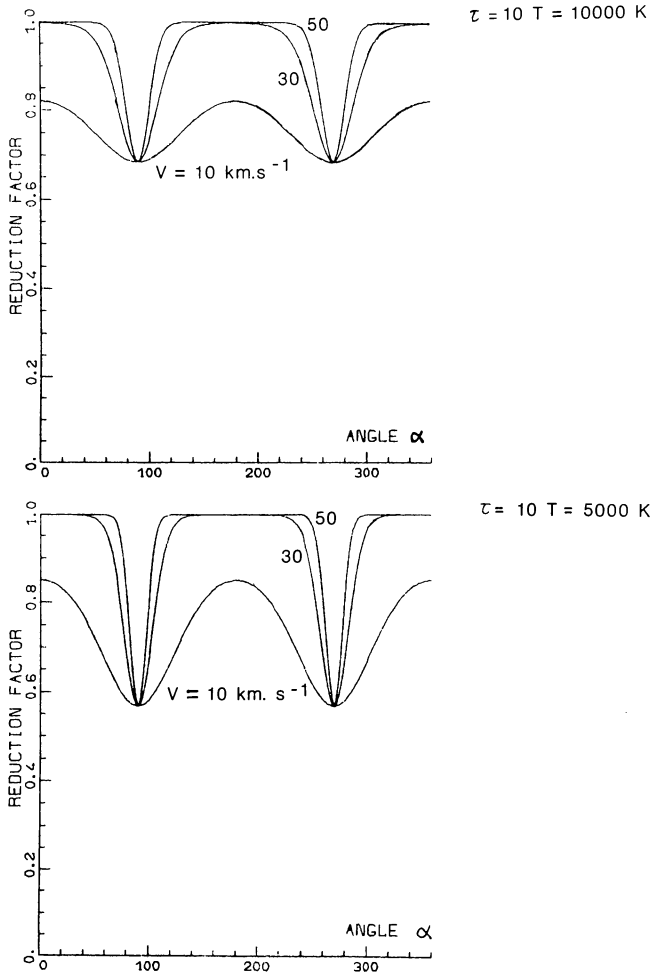

Fig. 6. The reduction factor is plotted as a function of angle α of the line of sight with the relative velocity vector V_R between the observer and the hydrogen flow, assumed to be at the uniform temperature $T = 10\,000$ K, for $V_R = 10$, 30 and 50 km s^{-1}. The minimum reduction factor is obtained for $\alpha = 90°$ (zero Doppler shift). For large values of V_R, the Doppler shift $_R \cos\alpha$ varies rapidly around $\alpha = \pi/2$

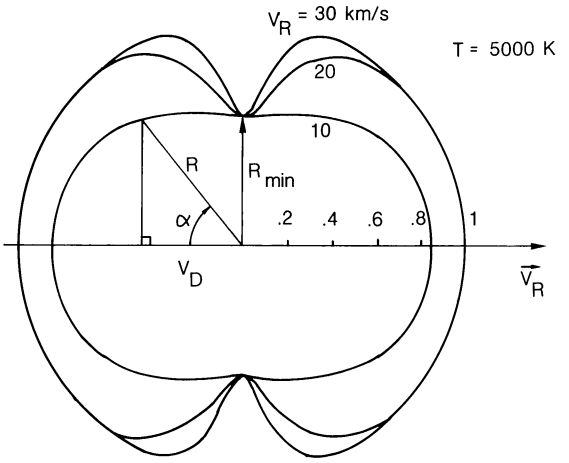

Fig. 7. The reduction factor R is plotted in polar coordinates (R, α), for $T = 5{,}000$ K and 3 values of V_R: 10, 30, 50 km s^{-1}. These curves are the meridian curves of the surface of revolution represented in Fig. 8

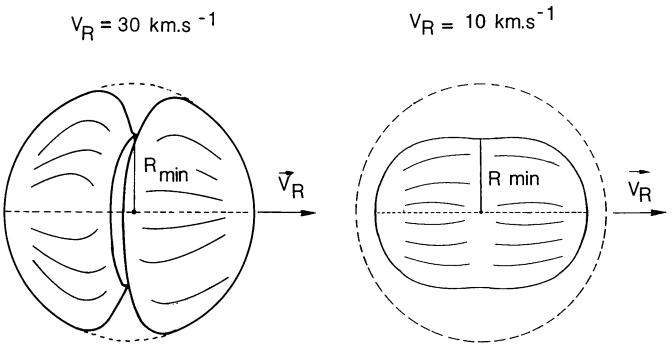

Fig. 8. When the reduction factor is mapped on the whole celestial sphere, the pattern of R has a symmetry of revolution around V_R. The meridian curve is displayed in Fig. 7 for $V_R = 10$, 30, and 50 km s^{-1}. In the plane perpendicular to V_R, the absorption is maximum (the reduction factor is minimum) along the zero Doppler shift circle (ZDSC). The absorption pattern looks like a "crunched apple"; the width of the crunch depends on the velocity V_R

A typical angular width of the absorption region $\Delta\alpha = \pi/2 - \alpha_t$ may be defined by the angle α_t for which the absorption $1 - R_t$ is half the maximum absorption $1 - R_{\min}$:

$$R_t = \frac{1 + R_{\min}}{2}. \tag{9}$$

Since the line width of the emission line $\Delta\lambda_e$ is connected to the temperature T:

$$\Delta\lambda_e = (\log^2)^{1/2} \frac{\lambda_0}{c} \left(\frac{2kT}{m}\right)^{1/2}$$

the angular width $\Delta\alpha$, the temperature T and the module of V_R are connected by an approximate relationship:

$$V_R \sin(\Delta\alpha) \approx \left(\frac{2kT}{m}\right)^{1/2}. \tag{10}$$

The results of Fig. 6 have been also plotted in a polar coordinates system (R, α) in Fig. 7. Each of them is the meridian curve of the surface of revolution of the R pattern as seen from different situations in the solar system. The R pattern is a sphere of radius unity, "crunched" like an apple along the ZDSC plane in the region where the H cell has a substantial effect (Fig. 8).

Let us assume a wind velocity V_w of 20 km s^{-1} in the ecliptic plane, in the direction defined by the ecliptic longitude $l_e = 270°$ for illustrative purposes, and an earth orbiting spacecraft. The three curves of Fig. 6 correspond to three typical locations of the Earth, at $\lambda = 0°$ ($V_R = 10$ km s^{-1}), $\lambda = 180°$ ($V_R = 50$ km s^{-1}), and $\lambda = 90°$ ($V_R = 36$ km s^{-1} instead of $V_R = 30$ km s^{-1}). The shapes of the R pattern are illustrated on Figure 8 for two velocities 10 and 30 km s^{-1}. When the velocity V_R is small, 10 km s^{-1} for instance, there is some absorption in all directions, and the R pattern would look like a "peanut" rather than an apple.

We can then summarize how the interstellar gas parameters can be determined from one single mapping of the R pattern of the complete celestial sphere with the Doppler angular spectral scanning method, in the presently studied uniform gaussian case:

1. Minimum values of measured R are distributed along a great circle of the celestial sphere (the ZDSC). The direction of $V_R = V_s + V_w$ lies along the axis of this great circle.

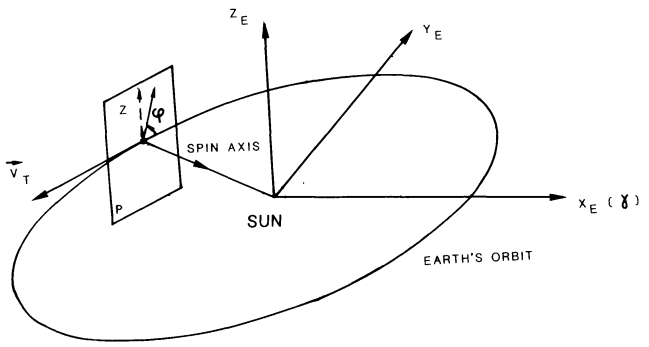

Fig. 9. Geometry of observations conducted with Lyα photometers on Prognoz 5 and Prognoz 6. The spin axis of the spacecraft is oriented towards the sun. The scanning plane P is perpendicular to the spin axis and contains the Earth's orbital velocity V_T. In the plane P, a direction of sight is defined by angle ϕ with vector $-V_T$. The North ecliptic pole (Z axis) is at $\phi = \pi/2$

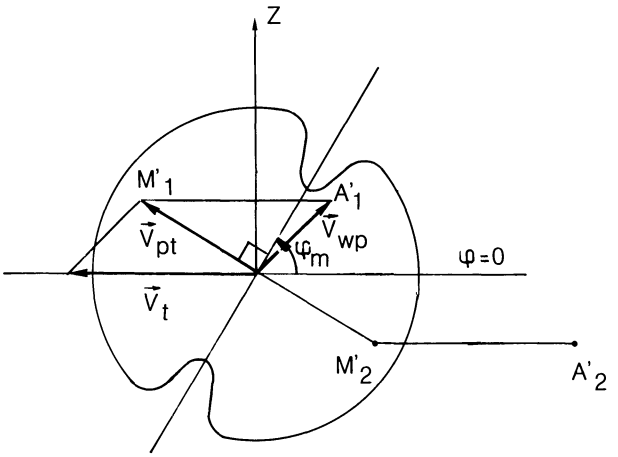

Fig. 10. The distribution of reduction factor R shows two minima $R_{\min}$ at angle $\phi_m (O \leqq \phi_m \leqq \pi)$ and angle $\phi_m + \pi$, where the P plane crosses the ZDSC plane. Therefore the projection $V_{PT} = V_{wP} + V_T$ on the plane P of the relative vector $V_w + V_T$ is at right angle with ϕ_m (no Doppler shift). The legnth of V_{PT} is obtained from the width of the absorption region. There are two possible determinations for the end of vector V_{PT}, M'_1 and M'_2 and by subtraction of V_T two possible determinations of V_{wP}, A'_1 and A'_2, corresponding to a positive or negative component of V_w on Z axis, $V_w(Z)$. The point A'_1 is defined as the correct determination for the projection of V_w on plane P in this figure

2. The value of $R_{\min}$ directly determines the temperature T, assuming there is no background radiation in the bandwidth of the detector.

3. The module of V_R is determined from the angular width $\Delta\alpha$ of the absorption region along the ZDSC.

4. The vector V_R is determined; since V_s is known, the vector $V_w = V_R - V_s$ is therefore determined.

In fact, since there is a complete symmetry of the Doppler shift effect on absorption about $\lambda - \lambda_0 = 0$, the direction of V_R is not completely determined, and could be in one direction or in the reverse direction along the ZDSC axis. Two values of V_w are possible. To be completely rigorous, a second mapping of the R pattern would be required with a different situation of V_s in the solar system to solve completely the problem.

4. Doppler angular scanning in a plane

In this section we consider the particular geometry of observations of Prognoz 5 and 6. Instead of a complete celestial mapping, measurements were recorded along a great circle in a single plane, perpendicular to the Sun-Earth line (Fig. 9). Still, all parameters of the interstellar wind can be determined from observations, as will be explained below. This situation deserves some special consideration, since many spacecrafts are spin stabilized with the spin vector oriented toward the sun.

In the scanning plane P, the direction of sight is defined by the angle ϕ, with the origin of angles in the ecliptic plane, opposite to the Earth's velocity V_T, lying at $\phi = 180°$. This scanning plane cuts the ZDSC along a line at angles $\phi = \phi_m$ and $\phi = \phi_m + \pi (0 \leqq \phi_m \leqq \pi)$. The absorption pattern is represented on Fig. 10 in polar coordinates, with two regions of absorption ($R \leqq 1$) centered along this line.

The reduction factor has a minimum value $R_{\min}$ which corresponds to a temperature T given from Fig. 5 (with $V_D = 0$) and Eq. (8). This minimum value is obtained for $\phi = \phi_m$, where the Doppler shift is zero. Therefore, the projection V_{PT} of $V_R = V_w + V_T$ on the scanning plane is lying at $\phi = \phi_m + \pi/2$. Let V_{wP} be the projection of V_w on the scanning plane P. The vector V_{PT} is $V_{wP} + V_T$ since V_T is in the plane P.

For any direction ϕ, the Doppler velocity V_D in the line of sight is $V_D = V_{PT} \sin(\phi - \phi_m)$.

Therefore, once the temperature has been determined, measured values $R(\phi)$ and curves of Fig. 4 can be used to determine V_D, and the length V_{PT} of the vector V_{PT}:

$$V_{PT} = \frac{V_D}{\sin(\phi - \phi_m)}. \tag{11}$$

All values $R(\phi)$ should give the same value of V_{PT}, which determines the "velocity" at which the Doppler angular scanning in the plane P is made. If V_{PT} is large, the absorption region is narrow. If V_{PT} is small, the absorption region is wide.

Once the length of V_{PT} is determined, the projection V_{wP} of V_w on plane P is also determined. There is still one difficulty, because there are in fact two possibilities of direction for V_{PT}, which could also lie at $\phi = \phi_m - \pi/2$. The "good choice" is imposed by the projection of V_w on the Z ecliptic axis. Therefore, when the spacecraft is moving along the Earth's trajectory (with ecliptic longitude λ), the "good choice" will be either always $\phi = \phi_m + \pi/2$ or always $\phi = \phi_m - \pi/2$.

Let us assume that it is possible to select one of the two determinations. Then we can derive the Z component of V_w, $V_w(Z)$, and its component $V_w(\lambda)$ along the axis $\phi = 0$:

$$V_w(Z) = V_{PT} \mathrm{Cos}\, \phi_m, \tag{12}$$

$$V_w(\lambda) = -V_{PT} \sin\phi_m + V_T \quad (V_T = 30\,\mathrm{km\,s^{-1}}). \tag{13}$$

From several observations at various positions of Earth, the vector V_w can be completely determined. Let $OXYZ$ be the ecliptic coordinates system. The plane P (which contains vectors) can be translated to axis OZ for clarity. When the ecliptic longitude of the Earth ε changes, plane P will rotate around OZ axis. As illustrated

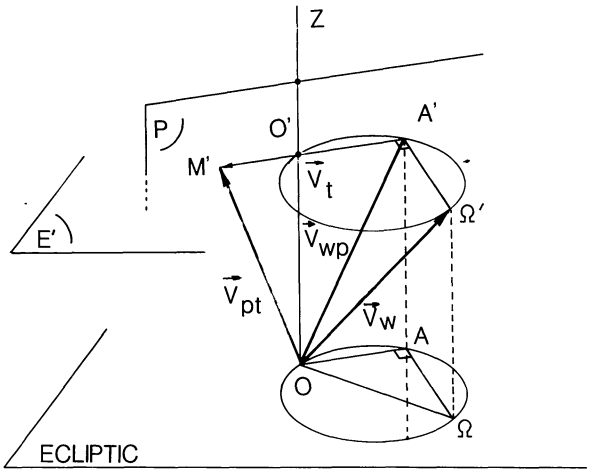

Fig. 11. The scanning plane P is now represented passing through OZ axis, in the velocity space. The plane E' is parallel to the ecliptic plane E at altitude $V_w(Z)$, and contains the point Ω', extremity of vector V_w, and its projection A'_1 (A' on the figure) on plane P. When the Earth moves, the plane P is rotating around OZ and A'_1 describes a circle of diameter $O'\Omega'$. The same is true for O, A and Ω, projections of O', A'_1, and Ω' on ecliptic plane. All lines perpendicular to A'_1 intersect each other at Ω'_1 whereas lines perpendicular to the wrong determination A'_2 do not intersect

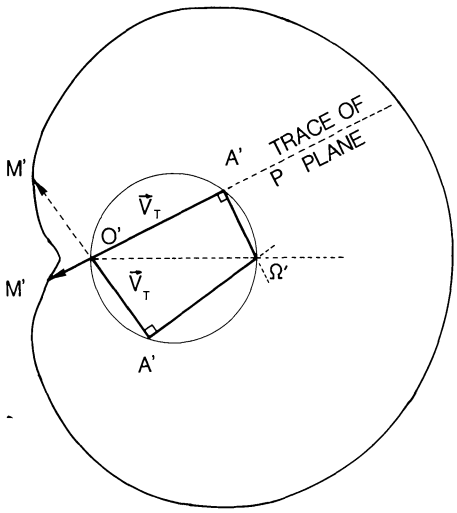

Fig. 12. Vector configuration in the ecliptic plane. The point Ω' is found at the intersection of three lines perpendicular to A' for three positions of the Earth (orientation of plane P). Only two are represented here for clarity. The locus of M', defined on the preceding figure as the projection of $V_w + V_T$ on P, describes a conchoid of circle since $\overline{O'M'} = \overline{O'A'} + \overline{A'M'}$, $\overline{A'M'} = V_T = 30$ km s^{-1}. Here $O'\Omega' = 25$ km s^{-1}

on Fig. 11, the end of vector V_w is at point Ω' and its projection on OXY at point Ω. Along the line D the point Ω' is projected on point A' in the P plane (and Ω is projected on A). Since, as was seen above, the point A', end of vector V_{wP}, can be determined from R measurements in plane P, it follows that the point Ω' will be located at intersection of all lines D perpendicular at A' to different planes P corresponding to different positions of the Earth in the solar system.

Figure 12 illustrate the situation projected on the ecliptic plane OXY, and also in the plane E' parallel to ecliptic plane OXY, passing through the end of vector V_w (Fig. 11). The point A, projection of V_{wP}, is located on a circle which diameter is $O\Omega$, whereas the point A' describes a similar circle in the plane E'.

If M' is the end of vector V_{PT}, also lying in the plane E', the locus of points M' when ε changes is a curve determined by the relation $\boldsymbol{O'M'} = \boldsymbol{O'A'} + \boldsymbol{V_T}$, where V_T has a constant magnitude. Since $\boldsymbol{O'A'}$ describes a circle of diameter $\boldsymbol{O'\Omega'}$, M' describes a conchoïd of a circle, illustrated on Fig. 12. In the particular case where $\boldsymbol{O'\Omega'}$ would also be of 30 km s^{-1}, the locus of M' would be a cardioïd.

It was here assumed that the sign of the Z component, $V_w(Z)$ is known. In fact, what should be done to discriminate the good choice is to try the two determinations of point A': A'_N (if the sign is positive) and A'_S (if the sign is negative). If the determination which corresponds to reality is selected, all lines perpendicular to scanning planes P will cross each other at a single point Ω', and the point A' will describe a circle of diameter $\boldsymbol{O'\Omega'}$. On the contrary, it can be easily demonstrated that, if the wrong determination is selected, the point A' will describe a conchoïd of circle and all lines will not intersect each other.

It can be useful to derive the angle ϕ_m from equations (11) and (12), and with the expression of the ecliptic component $V_w(E)$ of the wind. Since $V_w(\varepsilon) = V_w(E)\cos(\varepsilon - \varepsilon_w - \pi/2)$, where ε_w is the ecliptic longitude of the wind direction, it can be derived that:

$$\operatorname{tg}\phi_m = \frac{V_w(E)\sin(\varepsilon_w - \varepsilon) + V_T}{V_w(Z)}. \tag{14}$$

In summary, the following strategy is to be followed for the particular geometry of a single scan plane perpendicular to the Earth-Sun line at various positions of the Earth:

1. The minimum value of the reduction factor $R_{\min}$, found at angle ϕ_m indicates the temperature of the interstellar wind.
2. The projection of $V_w + V_T$ on the plane is at right angle of ϕ_m.
3. The module of this projection is found from the angular extent of the absorption region, and the projection A' of V_w on the plane P is determined (two possibilities for A').
4. With three different positions of the Earth, the vector V_w is completely determined.

5. The problem of galactic background

In this section, we consider the effect of the presence of a possible galactic background on our geometrical method in the uniform gaussian case.

Up to now we have made the assumption that the only signal detected in the wavelength bandwidth of the photometer, of the order of 100 Å, is the interplanetary Lyα emission I_0. If there is a weak continuum of galactic background, it will not be affected by the absorption of the H cell, which is very narrow in wavelength but will be integrated by the photometer, without discrimination whatever is the status of the hydrogen cell, ON or OFF.

There are two potential sources of galactic background in the wavelength region around Lyα, 1216 Å. One is the diffuse galactic background observed in the UV at larger wavelength, $\lambda = 1690$ Å (Joubert et al., 1983), thought to be the result of scattering by dust grains of the stellar UV flux (with some possible minor extragalactic contribution). The measured flux at $\lambda = 1690$ Å is in the range 500–2000 photons (cm^2 s Å ster)$^{-1}$, or $\simeq 0.5$ to $2\,10^{-2}$ Rayleigh/Å and should not contribute substantially to the signal detected around Lyα in a 100 Å bandwidth.

The other potential source is Lyα emission, which originates from stellar photons (mainly O and B stars) scattered by H atoms in the interstellar medium. The huge optical thicknesses involved

imply that the spectral profile would be very wide, from the wing contribution, and imply also that this background would be isotropic.

The problem of radiative transfer has been considered by Thomas and Blamont (1976). These Lyα photons, experiencing many scatterings with H atoms, have a large probability to be absorbed by dust grains, and they concluded that the galactic Lyα background intensity should be less than 10 Rayleigh, while the interplanetary signal is more than 120 Rayleigh.

However, since there are up to now no measurements of the galactic background just around Lyα wavelength, we have to consider the possibility of a larger background, up to $\simeq 50$ Rayleigh, which is up to now the lowest experimental limit, derived by Bertaux et al. (1972).

Let us assume that there is a galactic contribution I_g of the continuum in the bandwith of the instrument, not completely negligible in respect to I_0. The measurement would be, when the cell is off, $I_m = I_0 + I_g$, and when the cell is activated, $I'_m = R_0 I_0 + I_g$.

The measured reduction factor R_m will be related to the reduction factor R_0 affecting the interplanetary intensity I_0 (which would be measured in absence of I_g) by:

$$R_m = \frac{R_0 I_0 + I_g}{I_0 + I_g}. \tag{15}$$

It means that R_m is larger than R_0, and, if interpreted as the result of the cell on a gaussian profile with the curve of Fig. 5 for $V_D = 0$, will yield an "apparent" temperature T_m larger than the true temperature of the gas, T_0. Even a low value of 10 Rayleigh for I_g would induce a temperature difference $T_m - T_0 \simeq 1000$ K in the direction where $I_0 = 120$ Rayleigh.

The excess of temperature increases with galactic contribution and thus, assuming I_g is approximately isotropic, T_m will be larger for lines of sight directed to the downwind ionization cavity, where intensity I_0 is lower and the ratio I_0/I_g is larger. Therefore, if the measured temperature T_m, interpreted with the assumption $I_g = 0$, is different with different directions, it may be the signature of the presence of a galactic background. But, as it is shown in the companion paper (Lallement et al., 1984, this issue), other effects can also present the same kind of signature.

We now describe a geometrical method which allows to determine the vector V_w, even in the presence of a galactic background I_g from three sets of measurements in three different planes. Considering that the Lyα galactic background is expected to be highly isotropic, it will be assumed that the spatial gradient $dI_g/d\phi$ is negligible in respect to the interplanetary gradient $dI_0/d\phi$.

The only measurement needed for our method is the angular position ϕ_m of maximum absorption (minimum reduction factor) of the interplanetary emission I_0, indicating the direction where the Doppler effect is zero in the scanning plane. If there is a galactic background I_g, the measured position ϕ'_m of the measured minimum reduction factor $R_{\min}$ will be different from $\phi_m \cdot \phi'_m$ will be displaced from the direction ϕ_m towards the direction of larger intensities. The reason is that the increase in the ratio I_0/I_g leading to a larger absorption, compensates for the smaller absorption induced by a shift from the center of the gaussian line.

The displacement $|\phi'_m - \phi_m|$ is zero when $dI_0/d\phi = 0$, and is an increasing function of $|dI_0/d\phi| = |dI_m/d\phi|$. As the data shown in the companion paper demonstrate, for the observations for which $|dI_m/d\phi|$ has its largest value (worst case), the displacement $|\phi'_m - \phi_m|$ is $\leqq 2$ degrees even if the ratio I_g/I_0 amounts to the very large value of 0.9. For the other periods of observations, the region of maximum absorption coincides with a maximum of I_m and the displacement is totally negligible. Therefore, we will ignore this very small displacement effect in all cases (any way lower than the measurements uncertainties) and will consider that the measured direction ϕ'_m of the minimum reduction factor $R_{\min}$ indicates the direction ϕ_m of the ZDSC, perpendicular to the relative vector $V_R = V_T + V_w$.

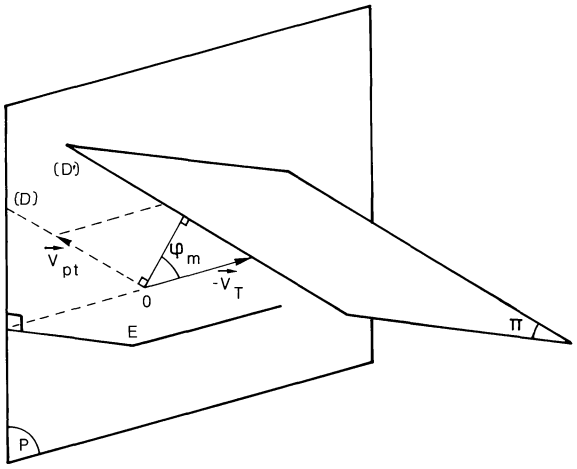

Fig. 13. Illustration for a geometrical method to determine the wind velocity vector V_w applied even in presence of a galactic background contribution. Whatever is the background the extremity of vector V_{pt} (projection on the scan plane P of the relative velocity vector $V_R = V_w + V_T$, where V_T is the earth's velocity) is on a line (D) normal to the direction of maximum absorption $\phi = \phi_m$. Thus the extremity of V_{wP} (projection of V_w on the scan plan P) is on the line (D') obtained from (D) by a translation of the vector $-V_T$. The extremity of V_w is in a plane (π) normal to the scan plane (P) which intersects with (π) along D'. The plane (π) is represented as viewed from below. The ecliptic plane is E. At every scan plane P corresponds such a π plane. The common intersection of all planes π is the extremity of V_w

The geometric method is presented in Fig. 13, which represents the plane of observation perpendicular to the Sun-Earth line. In this plane, V_T is known, and the direction of V_{PT} (projection of $V_T + V_w$ on the scanning plane P) is determined at $\phi = \phi_m \pm 90°$, on a line D.

Therefore, it means that the projection V_{wP} of V_w on the P plane is on a line D', parallel to the line D, translated from D by the vector $-V_T$.

Consequently the extremity of V_w is in a plane π normal to the scan plane P, which intersects with π along the D' line. Such a plane π can be determined for each different scanning plane. All planes π will intersect each other at a common point which is the extremity of V_w.

The difference of this method with respect to the method described in Sect. 4 is that it uses neither the width of the absorption trough nor the knowledge of the temperature, but only the direction of maximum absorption. There is a small price to pay, however. In the first method, only two scan planes could be used, the third one being used to discriminate the sign of the latitude of V_w.

In the present method, three planes are absolutely necessary to determine V_w. But it is more general, since it works even if there is a galactic background, and it is used in the companion paper to yield a first estimate of the position of V_w.

Once the vector V_w is defined, there is a possibility to estimate what is the galactic contribution I_g to the total measured intensity.

Instead of considering the reduction factor $R(\Delta\lambda_D)$ of Eq. (6), let us consider the signal absorbed by the H cell which is purely of interplanetary origin, $I_a(\Delta\lambda_D)$:

$$I_a(\Delta\lambda_D) = I_m - I'_m = I_0 - R(\Delta\lambda_D)\, I_0 \qquad \text{or:}$$

$$I_a(x) = I_0 - I(x)$$

by replacing $\Delta\lambda_D$ by x and setting $I(x) = R(x)\, I_0$.

This signal can be safely attributed to the interplanetary Lyα, since it is absorbed by the H cell. $I(x)$ is the interplanetary signal which is transmitted by the cell:

$$I(x) = \int_{-\infty}^{+\infty} f(\lambda - x)\, T(\lambda)\, d\lambda \tag{16}$$

and

$$I_a(x) = \int_{-\infty}^{+\infty} f(\lambda - x)\, [1 - T(\lambda)]\, d\lambda \tag{17}$$

As a result of the Doppler angular scanning method are obtained a series of measurements. $I_a(x_i)$, which can be integrated over wavelength. The result is:

$$\int_{-\infty}^{+\infty} I_a(x)\, dx = \int_{-\infty}^{+\infty} \int_{-\infty}^{+\infty} f(\lambda - x)\, [1 - T(\lambda)]\, d\lambda\, dx$$

$$= \int_{-\infty}^{+\infty} [1 - T(\lambda)] \left(\int_{-\infty}^{+\infty} f(\lambda - x)\, dx \right) d\lambda$$

$$= I_0 \int_{-\infty}^{+\infty} [1 - T(\lambda)\, d\lambda]$$

$$\int_{-\infty}^{+\infty} I_a(x)\, dx = I_0\, W \tag{18}$$

where W is the equivalent width of absorption of the hydrogen cell.

In practice, the integral on $I_a(x)$ is limited to the range of $x = \Delta\lambda_D$ provided by the Doppler scan, and here we assumed that it is large enough to reach spectral regions where $f(\lambda)$ and $I_a(x)$ are negligible.

From Eq. (18) we derive immediately:

$$I_0 = \frac{\int I_a(x)\, dx}{W}$$

in which the equivalent width W is a known function of the fixed optical thickness τ ($W \simeq 30$ mÅ for $\tau = 10$), and an estimate of the galactic background I_g can be derived:

$$I_g = I_m - I_0$$

It can be noted that Eq. (18) holds, whatever is the spectral profile of I_0, if it is constant over the scanned region.

Here it was assumed for the sake of clarity that the intensity is uniform with direction. If I_0 is changing with the direction, an average on I_0 on the direction should be introduced in (18) instead of I_0 and an average on I_m should be introduced in the above equation.

This technique is applied in the companion paper (Lallement et al.).

6. Discussion

In this paper we have exposed the technique of Doppler angular spectral scanning (DASS) applied in the simple case of a uniform gaussian profile. Either in the case of a full sky mapping or in the case of a single scan plane, repeated at various positions in the solar system, measurements are highly redundants, since four parameters (V_w, T) are to be derived from a large number of measurements. For instance, the value $R_{\min}$ should always be the same, along the ZDSC and at any place in the solar system.

The shape of the absorption region, $R(\phi)$, can be strictly predicted with only one parameter, V_D, once $R_{\min}$ and T are derived (if there is no galactic background).

It follows that, if some non-random deviations are found between measurements obtained from a space experiment and the simple gaussian case, these deviations indicate that the reality is different from the simple model.

It may depart from the model in two different respects: either there is a significant galactic background, or the velocity distribution cannot be represented by a uniform gaussian, or even a combination of both causes.

As it was shown in Sect. 5, our geometrical construction of the velocity vector V_w with intersection of planes π is independant of the existence of a galactic background. Therefore, if all planes π do not intersect with one another, this cannot be explained by the presence of a galactic background, which does not modify their positions. Indeed, this is what happens when this π plane method is applied to the results of Prognoz, as it is described in the companion paper. This is an evidence that the velocity distribution of interstellar H atoms in the solar system cannot be represented by a uniform gaussian.

One important factor of departure is the unbalance between solar gravitation F_g and Lyα solar radiation pressure F_r. For the gaussian case, we have assumed that $\mu = F_r/F_g = 1$, whereas the solar Lyα flux is known to change substantially with the eleven year solar cycle. When $\mu \neq 1$, individual trajectories are no longer straight lines, and the velocity distribution is modified. The first measurements with the absorption cell Lyα photometer on board Prognoz 5 were made in 1976 (Bertaux et al., 1977). From the analysis of the distribution of R in a plane perpendicular to the Sun Earth line, a value $R_{\min} = 0.68 \pm 0.01$ was found, from which was derived directly a temperature $T = 8.8 \pm 1\ 10^3$ K (including an uncertainty of 10% on τ). But this value of T was derived assuming the simple case of $\mu = 1$ and a gaussian profile, whereas for the low solar activity of 1976, a value of $\mu \leqq 1$ would have been probably more appropriate. Indeed, Wu and Judge (1980) computed the exact velocity distribution assuming a value of $\mu = 0.75$ and the particular position of Prognoz at the time of measurements (1 December 1976). They found that, for this particular downwind position, the velocity distribution was widened in respect to the unperturbed Maxwell Boltzmann distribution at infinity. The measurement of $R_{\min} = 0.68$ (which is essentially a linewidth measurement) should according to their computation, correspond rather to a temperature at infinity of $T = 7000 \pm 1200$ K.

The solar ionization is another factor of modification of the velocity distribution (Wu and Judge, 1979; Lallement, 1983). Atoms which spend more time near the sun are more likely to be ionized by solar wind charge exchange and EUV photons. Faster atoms are less ionized than slower atoms. Globally, the ionization can either narrow or widen the velocity distribution, depending on position in the solar system in respect to the gas flow vector V_w.

All these effects can be modelled and will be studied systematically in a future work (Lallement, Bertaux, and Dalaudier, in preparation). Indeed, since measurements are numerous, one can hope to extract from them two additional parameters: μ and the lifetime of one H atom versus ionization. The strategy of analysis will be slightly different from what has been exposed in the present simple case of a gaussian profile. In this more complicated

situation, all parameters cannot be retrieved directly from the absorption measurements. One has to compare computed and measured curves $R(\phi)$ to derive a "best fit" set of parameters. However, we will still have to deal with curves $R(\phi)$ of the reduction factor as a function of scan angle ϕ, and it was felt that it was necessary for educational purposes to explain first in some details the significance of such curves in the simple case of a non-modified Maxwell-Boltzmann velocity distribution.

Perhaps it should be reminded at this stage that the DASS method allows to analyze a Lα *line profile* (even if it is different from a gaussian), which is an integrated quantity along a line of sight, and does not give access to the details of the velocity distribution at the various points along the line of sight. In order to produce a diagnostic from the Lα line profile, one has to imply some additional assumptions, the simplest one being that, in a first approximation, the interstellar gas velocity distribution is not modified by the heliosphere, giving a uniform gaussian profile. In other cases, it can still be remarked that the integral along the line of sight is weighted according to the emissivity function, which is the product of density by solar flux excitation decreasing as r^{-2}. There is a maximum of this function along each line of sight, which gives the maximum contribution to the Lα line profile.

In the companion paper (Lallement et al., this issue), the geometrical method described here is applied to five sets of Prognoz measurements. A first estimate of T and V_w can be derived, but there are systematic deviations in the measurements showing that the velocity distribution of interstellar hydrogen atoms is modified by the solar environment. Instead of being a simple assumption in the theoretical work of Wu and Judge (1980), it becomes an observed effect with Prognoz results.

Finally, it could be worthwhile to point out that the situation we have described in this paper is not unique in astrophysics.

There is a strong similarity of situation between the flow of interstellar hydrogen in the solar system and the cosmic background radiation at 3 K. In the first case, the spectroscopic study of the emission on the celestial sphere allows us to determine the relative velocity between the Sun and the hydrogen flow, thanks to the Doppler effect. In the second case, the Doppler effect has also been used to determine the motion of the Sun and of our Galaxy relative to the last scatterers of the microwave background (a motion named by Peebles (1971) the New Aetherdrift). Since the 3 k radiation is a continuum with a wavelength gradient, accurate measurements in a narrow frequency bandwith can be used to determine the Doppler effect. It is easy to show that the temperature $T(\theta)$ measured is:

$$T(\theta) = T_0\left(1 + \frac{v}{c}\cos\theta\right)$$

in which $T_0 = 3$ K is the mean cosmic radiation temperature, v is the velocity of the observer, and θ is the angle between the direction of motion and the line of sight (Gorenstein and Smoot, 1981). Indeed, from a series of measurements over the celestial sphere at 33 GHz on board a *U*-2 aircraft, Smoot et al. (1977) could determine that the Sun is moving at a velocity of $360 \pm 50\,\mathrm{km\,s^{-1}}$ in the direction 11.2 ± 0.5 h of right ascension and $19° \pm 8°$ declination. Substracting the $250\,\mathrm{km\,s^{-1}}$ circular motion of the Sun about our Galaxy, the Galaxy's motion relative to the background is found to be pointed within 33° of the Virgo Cluster, at a velocity of the order of $500\,\mathrm{km\,s^{-1}}$ (Gorenstein and Smoot, 1981). In this case of the 3° K cosmic background radiation, as well as in our case of the Lyα interplanetary background a Doppler angular scanning method is used to retrieve the relative motion of the sun with respect to the source of emission.

Appendix

Calibration of the H-cell optical thickness

The method which is used to measure at the laboratory the optical thickness τ of the H absorption cell was described in Mitchell and Zemansky (1934). The absorption of the H cell is measured on a Lyman α source which produces an emission line with a pure gaussian profile at room temperature. This is achieved with a high-voltage Lyman α discharge lamp, illuminating a resonance H cell. The resonance is observed at 90° from the incident light. Since velocity distributions projected on two perpendicular axis are independant in a Maxwell Boltzmann distribution, the resonance Lyman α line profile is a gaussian, whatever is the incident line profile.

Only a moderate heating of the tungsten filament (1 Watt) is necessary to achieve an optical thickness $\tau = 10$, which guarantees a long lifetime of the H cell (4 yr of operation of the H resonance cell on OSO-5, Vidal Madjar, private communication).

In flight, the geocoronal Lyα emission can be used as a "standard" natural source to check the stability of the H cell optical thickness τ.

The temperature of H atoms inside the cell is the temperature of the cell walls, because these H atoms are produced at the tungsten filament which is away from the light path. They suffer many collisions with H_2 molecules at a few Torr pressure before entering the light path. It was checked at the laboratory, by using a fine light pencil, that the optical thickness did not vary significantly over the ~ 1.5 cm width of the light path.

Finite angle of acceptance in the H cell

With the focusing lens as the entrance window, some light rays are tilted by an angle whose maximum value is $\simeq 8°$. Since the density of H is approximately uniform in the H cell, these photons will encounter an optical thickness slightly larger than the on-axis photons, by an amount $\theta^2/2$, which is less than 1 % and this effect is negligible.

Acknowledgements. We wish to thank Jean-Claude Lebrun for assistance on the computing system Cyber, kindly provided by Centre National d'Etudes Spatiales. We are indebted to Richard Toffolet who graduated from Ecole Polytechnique in 1979 and spent an efficient couple of months at Service d'Aéronomie on some aspects of the present work. We regret that he finally preferred to dedicate his marvellous abilities to the French Bridges and Roads system rather than to Astrophysics.

References

Adams, T.F., Frisch, P.C.: 1977, *Astrophys. J.* **212**, 300
Babichenko, S.I., Deregosov, E.V., Kurt, V.G., Romanova, N.N., Skljankin, V.A., Smirnov, A.S., Bertaux, J.L., Blamont, J.E.: 1977, *Space Sci. Instrumentation* **3**, 271
Bertaux,J.L., Blamont, J.E.: 1971, *Astron. Astrophys.* **11**, 200
Bertaux, J.L., Ammar, A., Blamont, J.E.: 1972, Space Research XII, 1559
Bertaux, J.L., Blamont, J.E., Tabarie, N., Kurt, V.G., Bourgin, M.C., Smirnov, A.S., Dementeva, N.N.: 1976, *Astron. Astrophys.* **46**, 19
Bertaux, J.L., Blamont, J.E., Mironova, E.N., Kurt, V.G., Bourgin, M.C.: 1977, *Nature* **270**, 156

Bertaux, J.L.: 1978, *Planetary Space Sci.* **26**, 431
Bertaux, J.L., Blamont, J.E., Marcelin, M., Kurt, V.G., Romanova, N.N.: 1978, *Planetary Space Sci.* **26**, 817
Blum, P.W., Fahr, M.J.: 1970, *Astron. Astrophys.* **4**, 280
Broadfoot, A.L., Kumar, S.: 1978, *Astrophys. J.* **222**, 1054
Dalaudier, F., Bertaux, J.L., Kurt, V.G., Mironova, E.N.: 1984, *Astron. Astrophys.* **134**, 171
Delaboudiniere, J.P., Carabetian, C.: 1975, *Space Science Instrumentation* **1,** 91
Delaboudiniere, J.P., Crifo, J.F.: 1976, *Space Research* XVI, p. 803
Delaboudiniere, J.P.: 1981, Thèse de Doctorat d'Etat, Université de Paris 7
Fahr, H.J.: 1974, *Space Sci. Rev.* **15**, 483
Fahr, H.J., Crifo, J.E., Wulf-Mathies, C., Seidl, P.: 1977, *Astron. Astrophys.* **58**, L21
Freeman, J., Bowyer, S., Paresce, F., Lampton, L.: 1976, *Rev. Sci. Instr.* **47**, 277
Freeman, J., Paresce, F., Bowyer, S., Lampton, L.: 1980, *Astron. Astrophys.* **83,** 58
Harris, D.L.: 1948, *Astrophys. J.* **108**, 112
Gorenstein, M.V., Smoot, G.F.: 1981, *Astrophys. J.* **244**, 361
Joselyn, J.A., Holzer, T.E.: 1975, *J. Geophys. Res.* **80**, 905
Joubert, M., Masnou, J.L., Lequeux, J., Deharveng, J.M., Cruvellier, P.: 1983, *Astron. Astrophys.* **128**, 114
Kumar, S., Broadfoot, A.L.: 1979, *Astrophys. J.* **228**, 302
Lallement, R.: 1983, Thèse de 3ème Cycle, Université P. et M. Curie
Lallement, R., Bertaux, J.L., Kurt, V.G., Mironova, E.N.: 1984, *Astron. Astrophys.* **140,** 243
Meier, R.R.: 1977, *Astron. Astrophys.* **55**, 211
Mitchell, A.C.G., Zemansky, M.W.: 1934, Resonance Radiation and excited atoms, Cambridge University Press
Peebles, P.J.E.: 1971, Physical Cosmology, Princeton: Princeton University Press
Ripken, H.W., Fahr, H.J.: 1983, *Astron. Astrophys.* **122**, 181
Smoot, G.F., Gorenstein, M.V., Muller, R.A.: 1977, *Phys. Rev. Letters* **39**, 898
Thomas, G.E.: 1972, Solar Wind SP-308
Thomas, G.E., Blamont, J.E.: 1976, *Astron. Astrophys.* **51**, 283
Thomas, G.E., Krassa, R.F.: 1971, *Astron. Astrophys.* **11**, 218
Wallis, M.K., Wallis, J.: 1979, *Astron. Astrophys.* **78**, 41
Weller, C.S., Meier, R.R.: 1974, *Astrophys. J.* **193**, 471
Weller, C.S., Meier, R.R.: 1981, *Astrophys. J.* **246**, 386
Wu, F.M., Judge, D.L.: 1979, *Astrophys. J.* **231**, 594
Wu, F.M., Judge, D.L.: 1980, *Astrophys. J.* **239**, 389